565

Small-angle neutron scattering by porous alumina membranes made of aligned cylindrical channels

Damien Marchal[a] **and Bruno Demé**[b]*

[a]*Laboratoire d'Electrochimie Moléculaire, UMR 7591, Université Paris 7 Denis Diderot - CNRS, 75251 Paris Cedex 05, France,* [b]*Institut Laue-Langevin, B.P. 156, 38042 Grenoble Cedex 9, France. E-mail: deme@ill.fr*

Small-angle neutron scattering is used to investigate porous alumina membranes (γ-Al_2O_3) made of parallel channels with cylindrical shape. The membranes are produced by anodization of thin aluminium sheets. The scattering experiments are performed in a coaxial geometry where the cylindrical pores are oriented with their long axis parallel to the incident beam resulting in isotropic scattering patterns due to the circular symmetry. The results obtained with commercial Anodisc® membranes and membranes synthesized in our laboratory are compared to radialy averaged 2D Fourier transforms of electron microscopy images of the alumina membrane surface and to known values of the materials' porosity.

Keywords: small-angle neutron scattering, porous alumina, cylinder, interface, structure factor, form factor

1. Introduction

Porous alumina films prepared by anodization of thin aluminium sheets are well known as filtration membranes for organic solvents and are available commercially. These films can be also synthesized at smaller scale using laboratory equipments for other applications such as the use as templates or as wave guides (Furneau *et al.*, 1989; Masuda *et al.*,1997).

Tailor-made alumina membranes have been synthesized for the development of microporous electrodes where the channels traversing the alumina membrane are connected at one end to a gold layer (Marchal *et al.*, 1997). The microporous part of the electrode (γ-alumina, Al_2O_3) is an isolating material to which thin lipid or polymer layers can be chemically grafted. If electron carriers can be embedded in the thin layer bound to the metal oxide and if the layer is continuous and defect-free from one side of the alumina membrane to the other, an additional dimension is given to the electrode that can provide information on diffusion coefficients of the electron carrier in the supported film (Marchal *et al.* 1998). This method can be applied to the study of electron transfer kinetics in reactions involving integral or peripheral membrane proteins in biological membranes (Marchal *et al.*, 2001).

In this paper we present results obtained by small-angle neutron scattering (SANS), electron microscopy and 2D Fourier analysis of EM images of unmodified alumina membranes. The geometry of the scattering experiment used here makes EM combined to 2D Fourier transforms a complementary tool to understand the porous structure of the material.

2. Materials and methods

2.1. Reagents

Aluminium foils, 1mm thick (Al 99.95 %) were from Merck (Darmstadt, Germany). 60 µm thick aluminium oxides were commercial inorganic membrane filter discs (Anodisc® 47 with a pore diameter of 200 nm) produced by Whatman (Maidstone, UK). Organic solvents were HPLC grade. Water with a typical resistivity of 18 MΩ was produced by the Milli-Q purification system from Millipore (Bedford, MA). Heavy water (99.9 % D) was provided by the ILL (Grenoble, France). All other chemicals were reagent grade.

2.2. Preparation of porous alumina membranes

Thin aluminium oxides were produced in the laboratory using the procedure first described by Miller & Majda (1986) and modified by Parpaleix *et al.* (1992). Briefly, aluminium oxide films were generated by anodization of aluminium foils at 65 V and 298 ± 0.5 K. Anodization under these conditions produces uniform aluminium oxide films with a pore diameter equal to 130 ± 20 nm and a thickness equals to 1-2 µm / h of anodization. Anodic films are separated from the aluminium substrate by immersion of the anodized foil in a saturated aqueous $HgCl_2$ solution. The films were extensively rinsed in water then immersed for 1 min in a 0.1 M NaOH solution to remove all traces of mercuric salt. Finally, the films were extensively rinsed in water and dried.

We prepared two different oxide samples with thicknesses of 3 µm and 10 µm. The specific area of the home made films is 16 ± 3 $m^2.cm^{-3}$ or 13.0 ± 2.5 $m^2.g^{-1}$ (Crawford *et al.* 1992; Marchal *et al.* 2002). Commercial, 60 µm thick aluminium oxides were directly used after extensive rinsing and removal of the polypropylene ring. Their specific area is 7.7 ± 0.8 $m^2.cm^{-3}$ or 6.4 ± 0.6 $m^2.g^{-1}$ (Crawford *et al.* 1992; Marchal *et al.* 2002).

2.3. Small-angle neutron scattering

SANS experiments were performed on D22 at the high-flux reactor of the Institut Laue-Langevin, Grenoble, France. Three settings were used to cover a q-range of $6x10^{-4}$ to $6x10^{-1}$ $Å^{-1}$, that is three orders of magnitude in reciprocal space (here, q is the modulus of the scattering vector, $q = 4\pi \sin\theta/\lambda$ with θ = half the scattering angle and λ = wavelength of the incident radiation). Data were corrected for the sample holder scattering and instrument background and normalized to a water calibration run for detector efficiency corrections and scaling to absolute units. A flat background was subtracted to account for the incoherent scattering of the sample. A 30 mm circular aperture was used at the collimation entrance (18.6 m before the sample) to improve resolution and to reduce the size of the virtual source compared to the full rectangular guide cross section of D22 (55 x 45 mm^2).

2.4. Sample orientation

The alumina sheets were hold fully hydrated between circular quartz windows and oriented in the beam as described previously (Marchal *et al.*, 2001). See also Auvray *et al.* (2000) and Pépy & Kuklin (2001). The experiment with membrane fragments oriented randomly was performed in a standard quartz QS Hellma cell.

2.5 Electron microscopy

The alumina films were coated with a thin layer of gold (5 Å) by sputtering. The images were acquired using a LEO S440 scanning electron microscope at an electron beam energy of 10 keV.

2.6 Fourier transforms of electron micrographs

2D Fast Fourier Transforms (FFTs) of electron micrographs were calculated using *Scion Image 4.0.2* based on *NIH Image* for MacIntosh by Wayne Rasband of National Institutes of Health, USA. It uses the 2D Fast Hartley Transform (FHT) routine (Bracewell *et al.*, 1986).

3. Analysis of small-angle scattering data

3.1 Scattering by cylinders

We focus here on the scattering by cylinders in coaxial geometry (pore long axis parallel to the incident beam). This geometry yields circular symmetry, that is isotropic patterns in scattering experiments.

The scattering by particles with spherical symmetry is given by the general relation:

$$I(q) = N(\Delta\rho)^2 V^2 P(q) S(q) \qquad (1)$$

where N is the number of particles per volume unit, $\Delta\rho$ the contrast, V the volume of the particles, $P(q)$ the particle form factor and $S(q)$ the structure factor.

For anisotropic particles with a strong aspect ratio like cylinders of length L and radius R oriented with an angle α between their long axis and the normal to the incident beam, the form factor was given by Fournet (1951):

$$P(q) = \int_0^{\pi/2} \left[\frac{2J_1(qR\sin\alpha)}{qR\sin\alpha} \frac{\sin\left((qL\cos\alpha)/2\right)}{(qL\cos\alpha)/2} \right]^2 \sin\alpha d\alpha \qquad (2)$$

where J_1 is the 1st order Bessel function of the 1st type. Eq. 2 simplifies to the scattering by a circular aperture in the case of perfect cylinders aligned in coaxial geometry ($\alpha = 90°$):

$$P(q) = \left[\frac{2J_1(qR)}{qR} \right]^2 \qquad (3)$$

From Eq. 2 it follows that the scattering by randomly oriented infinite cylinders also simplifies to the above relation.

Structure factors of parallel cylinders have been given by Oster & Ridley (1952). For pairs of infinite and random cylinders or pairs of cylinders in coaxial geometry the correlation function is given by:

$$S(q) = \frac{1}{4}\left[2 + 2J_0(2\gamma qR)\right] \qquad (4)$$

where J_0 is the zeroth order Bessel function of the 1st type, and γ a swelling parameter equal to $d/2R$ where d is the cylinder center-to-center distance. In a system composed of more than two correlated cylinders this relation is equivalent to considering only 1st neighbour correlations. In a system with higher order 1st neighbour and 2nd neighbour correlations can be considered using:

$$S(q) = \frac{1}{49}\left[7 + 24J_0(2\gamma qR) + 6J_0(4\gamma qR) + 12J_0\left(2\sqrt{3}\gamma qR\right)\right] \qquad (5)$$

for dilute, randomly oriented heptamers of parallel cylinders in a central 2D hexagonal arrangement.

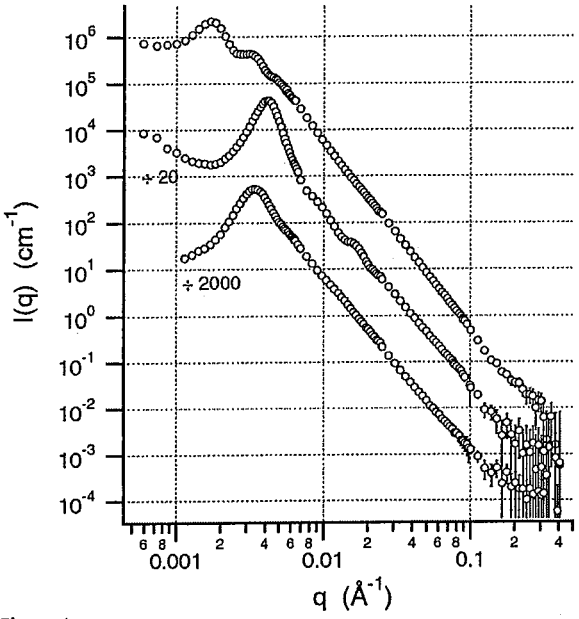

Figure 1
SANS by three different alumina membranes. Upper curve: Anodisc 200 from Millipore, mid and lower curves: 10 μm and 3 μm thick membranes synthesized in our laboratory. The upper curve is to the scale, the other are shifted by a factor indicated next to the curves.

3.2. Scattering by interfaces

Considering the porous structure of alumina membranes, another approach consists in considering the scattering produced by interfaces only. Owing to the pore diameter and to their center-to-center distance it is clear that far from the very low q range where these objects and their correlations are observed, the wide q region should be dominated by the interface scattering. This approach was used in a previous study to characterise the surface of the porous alumina membranes in the presence of supported model membranes (Marchal *et al.*, 2001). In the absence of interfacial structure, the scattering by a random interface defined by a step-like change of the scattering length density follows the Porod law (Porod, 1951):

$$I(q) = 2\pi\Sigma\frac{1}{q^4}(\Delta\rho)^2 \qquad (6)$$

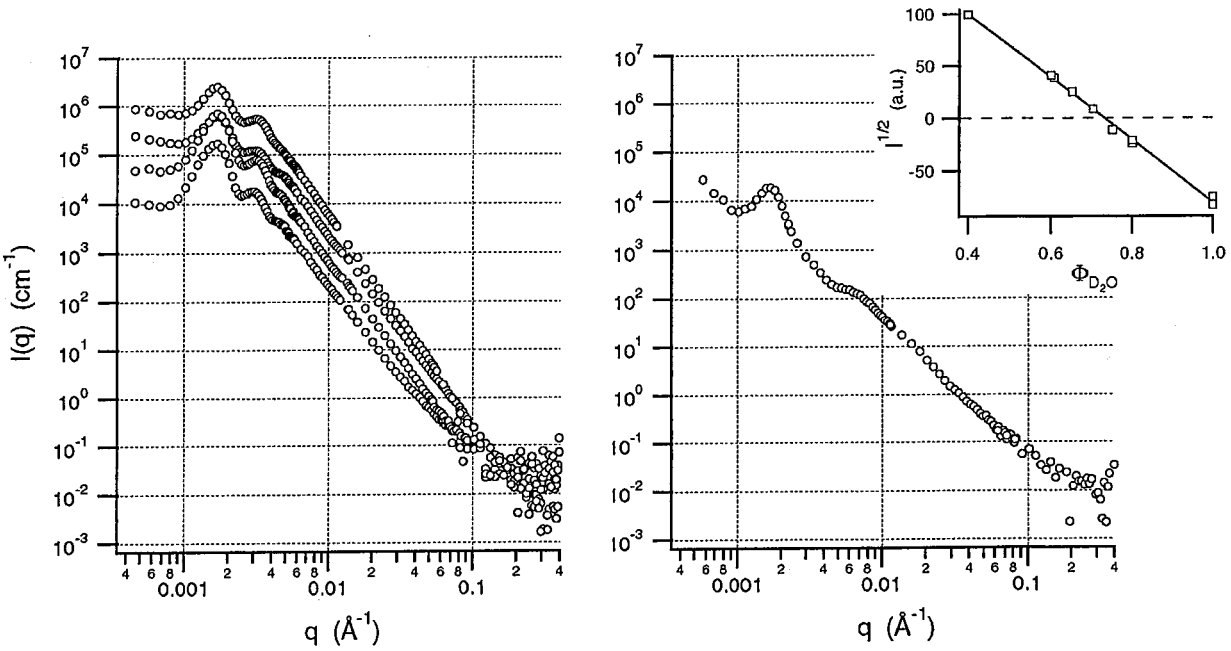

Figure 2
Left: SANS by an anopore membrane at various contrasts (from top to bottom: Φ_{D2O} = 0.80, 0.60, 1.00 and 0.40). Right: SANS at the average contrast match point (Φ_{D2O} = 0.731) determined from the linear fit to the data shown in the insert (values of $I^{1/2}$ are multiplied by -1 for Φ_{D2O} > 0.731 to linearise the I *vs.* Φ parabolic function).

This is only true at wide angles if long-range correlations due to defined shapes or interactions exist. In this case it is common to consider the wide angle signal by using:

$$\lim_{q\to\infty}\left[I(q).q^4\right] = 2\pi\Sigma(\Delta\rho)^2 \qquad (7)$$

For interfaces whose roughness can be represented in real space by a Gaussian function, a Debye-Waller factor can be used to account for the smooth change of scattering length density at the interface. In this case the scattering at wide angles decays faster than q^{-4} and Eq. 6 becomes:

$$I(q) = 2\pi\Sigma(\Delta\rho)^2\, q^{-4} \exp(-\sigma^2 q^2) \qquad (8)$$

where σ is the half width of the Gaussian function describing the interface location distribution relative to the mean position.

4. Results

4.1. Scattering by alumina membranes

Figure 1 shows the scattering of three different alumina membranes in D_2O: a 60 μm thick Anodisc 200 membrane, and two membranes synthesized in the laboratory with respective thicknesses of 10 μm and 3 μm. The very low-q signal is due to the large scale in-plane distribution of holes which has a 2D-pseudo-hexagonal order, characterized by the 1, √3, 2, ... sequence of pseudo-Bragg peaks. In the coaxial geometry used here, it is not expected to observe oscillations due to the longitudinal term of the cylinder form factor (Eq. 2) but the scattering should be sensitive to the radial term (the Bessel function) related to the circular section of the cylinders. Instead of the expected oscillations, we observe a wide power law decay that extends to wide angles.

At that stage one may wonder why the structure factor related to the cylinder position is observed and not the form factor of the channels. One tentative explanation lies on the fact that cylinders separated by a distance *d* (center-to-center) can have some polydispersity while *d* is a constant with less spread. We know from the synthesis process that the channels are initiated at given positions on the aluminium surface and that this is the step that determines the mean center-to-center distance between the channels, as well as its distribution. However, the pore radius results from a separated step of growth under aggressive chemical conditions that solubilise the metal oxide. So, due to these two separated steps *d* and *R* are two independent parameters.

4.2. Contrast match point of porous alumina

The scattering length density of alumina was measured by solvent contrast variation using D_2O volume fractions $\Phi(D_2O)$ ranging from 1 to 0.4. The series of scattering curves measured in this range of contrasts is displayed Fig. 2 (left). Fig. 2 (right) shows the scattering at the calculated average contrast match point (CMP) deduced from a linear fit to a $I^{1/2}$ *vs.* $\Phi(D_2O)$ plot shown in insert. The linear fit yields the zero contrast point for a volume fraction of 0.731 corresponding to a scattering length density $\rho = 4.50\times10^{-6}$ Å^{-2} close to the value reported recently for bulk alumina (Stefanopoulos *et al.*, 1999). However, this is slightly below the value expected for crystalline alumina if one considers the scattering length of γ-Al_2O_3 and its density. Using a density of1.25 g/cm^3 for the Anodisc 200 nm and a porosity of 39 %

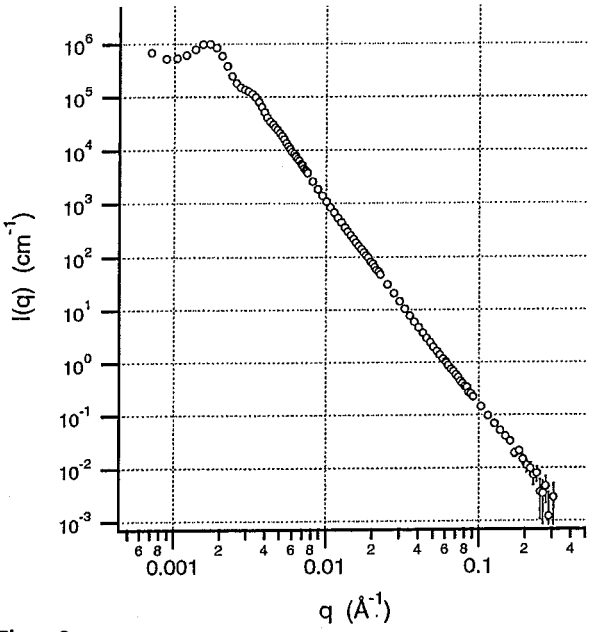

Figure 3
SANS by random fragments of an Anodisc membrane measured in D_2O.

(determined from EM images, Crawford *et al.*, 1992), we find a density of 3.2 g/cm^3 for bulk γ-alumina. Assuming the Anodisc as being composed of pure γ-Al_2O_3, these values lead to a scattering length density ρ_1 = 4.6x10^{-6} Å^{-2} in good agreement with the measured value. The slight difference between the experimental value and the calculation may originate from the uncertainty on the porosity determination or to the presence of impurities in the alumina, like the presence of hydroxyl groups that reduce the scattering length density of the material. Note that at the calculated CMP the intensity has not completely vanished indicating the presence of density fluctuations in the aluminium oxide. Fig. 3 shows the scattering by randomly oriented fragments of Anodisc 200 membrane. As in the case of the alumina membrane oriented in coaxial geometry, randomly oriented cylinders produce an isotropic pattern. Its radial average shown in Fig. 3 shows the same scattering behaviour with the low-q oscillations related to the pore correlations followed by the wide q^{-4} Porod behaviour. The specific area of alumina calculated in this geometry is reduced by a factor 5 compared to the coaxial geometry. This confirms the gain in intensity resulting from the orientation of the interface parallel to the beam.

4.3 Electron microscopy of alumina membranes

Electron micrographs of alumina membranes are shown in Fig. 4 (home made: A and B, Anodisc: D and E). Fourier transforms of images 4A and 4D are given in 4C and 4F respectively. Fig. 4G shows radialy averaged data of the 2D Fourier transforms. The mean center-to-center distances obtained from both neutron experiments and Fourier analysis of EM images are compared in Table 1. They are calculated according to:

$$d = \frac{4\pi}{\sqrt{3}} \frac{1}{q_{10}} \qquad (9)$$

where q_{10} is the position of the first Bragg reflection of the 2D pseudo-hexagonal arrangement of the cylinders.

5. Discussion

In Figs. 1 and 2, no oscillations of the Bessel function (the radial term of the cylinder form factor) are visible and a characteristic q^{-4} decay follows the hexagonal structure factor. It extends to the wide angle region indicating a perfectly smooth

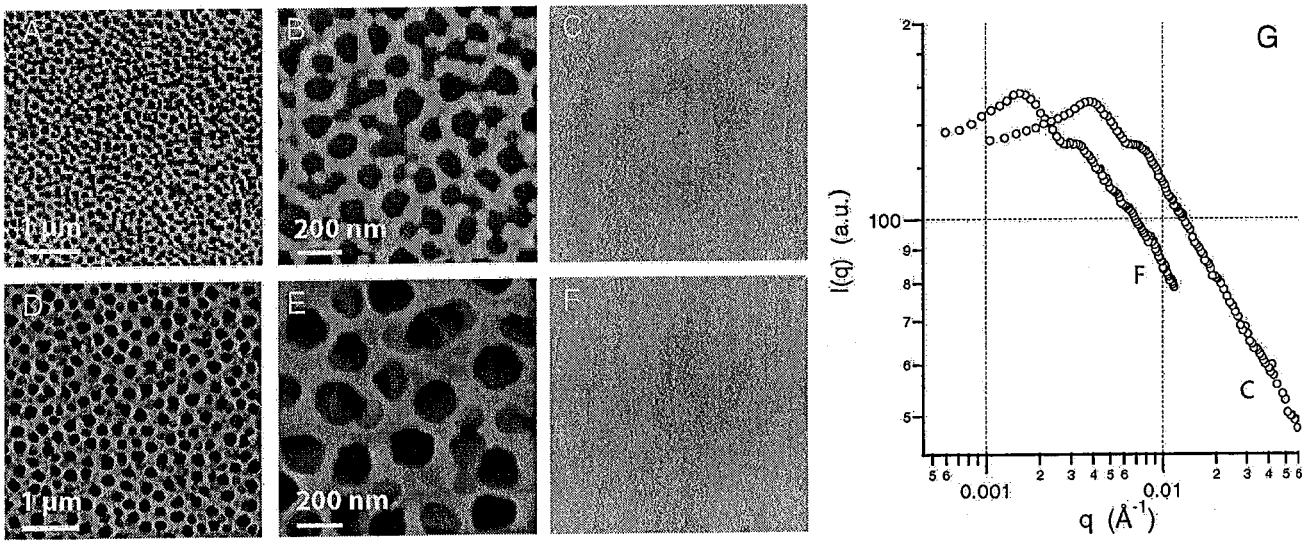

Figure 4
EM images of alumina membranes and corresponding 2D Fourier transforms (A, B, and C: home made membrane, D, E, and F: commercial Anodisc). G: radial averages of the Fourier transforms shown in C and F.

Table 1
Center-to-center distances *d*, cylinder radii *R*, and specific area Σ, obtained for the three alumina membranes by SANS and electron microscopy. FTEM means data resulting from the analysis of 2D Fourier transforms of electron microscopy images. Specific area determined by SANS are apparent values "boosted" by the orientation of the interface parallel to the beam.

thickness µm	Φ_{D_2O}	$\Delta\rho$ x 10^6 Å^{-2}	*d* (nm)		*R* (nm)	Σ ($m^2.cm^{-3}$)		Σ ($m^2.g^{-1}$)	
			SANS	FTEM	EM	SANS	EM	SANS	EM
60	0.4	2.04	435	400 ± 50	125 ± 25	493	8 ± 1	411	6.6 ± 0.8
	0.6	0.90	433			560		467	
	0.8	-0.48	439			515		429	
	1	-1.87	432			433		361	
10	1	-1.87	175	190 ± 30	65 ± 10	1120	16 ± 2	933	13 ± 2
3	1	-1.87	210	190 ± 30	65 ± 10	1120	16 ± 2	933	13 ± 2

interface. The data have been fitted according to Equation 8 in the exceptionally wide Porod regime observed for this material. The fitted parameters are the specific area of the sample Σ, and the roughness, while the contrast is known from the contrast variation experiment. Results of the fit to the scattering curves of Figures 1 and 2 are reported in Table 1.

If one refers to the known specific area of Anodisc 200 nm membranes (7.7 $m^2.cm^{-3}$) (determined from EM images, Crawford *et al.*, 1992), a boosting of the scattering by a factor of *ca.* 50 results from the coaxial orientation of the interface (see Table 1). Specific areas extracted in this configuration are thus apparent since the proportion of interface yielding a reflection and contributing to the q^{-4} law is artificially increased compared to a random interface (*e.g.* like in suspensions of spheres, vesicles, randomly oriented rods, etc.).

6. Conclusion

Scattering by alumina membranes is not only interesting because of their potential use as hosts for confined structures or as templates, but as they are model objects to understand the scattering by well aligned correlated channels with cylindrical shape.

Fourier transforms of electron micrographs is an interesting and complementary tool to scattering experiments when the problem can be simplified to the scattering by 2D objects like in the case of cylinders aligned in coaxial geometry.

References

Auvray, L., Kallus, S., Golemme, G., Nabias, G. & Ramsay J.D.F. (2001). *Stud. Surf. Sci. Catal.* **128**, 459-466.
Bracewell, R. N. (1986). The Hartley Transform. New York: Oxford University Press.
Crawford, G. P., Steele L. M., Ondris-Crawford R., Iannacchione, G. S., Yearger, C. J., Doane, J. W., Finotello, D. (1992). *J. Chem. Phys.* **96**, 7788-7795.
Fournet, G., (1951). *Bull. Soc. Fr. Mineral. Crist.* **74**, 37-172.
Furneau, R. C.; Rigby, W.R.; Davidson, A.P. (1989). *Nature*, **337**, 147-149
Masuda, H., Yamada, H., Satoh, M., Asoh, H., Nakao, M. & Tamamura, T. (1997). Appl. Phys. Lett., **71**, 2770-2773.
Marchal, D., Boireau, W., Laval, J.-M., Moiroux, J. & Bourdillon, C. (1997). *Biophys. J.* **72**, 2679-2688.
Marchal, D., Boireau, W., Laval, J.-M., Moiroux, J. & Bourdillon, C. (1998). *Biophys. J.* **74**, 1937-1948.
Marchal, D., Pantigny, J., Laval, J.-M., Moiroux, J. & Bourdillon, C. (2001). *Biochemistry*, **40**, 1248-1256.
Marchal, D., Bourdillon, C. & Demé, B. (2001). *Langmuir* **17**, 8313-8320.
Miller, C.J. & Majda, M. (1986) *J. Am. Chem. Soc.* **108**, 3118-3120.
Oster, G. & Riley, D. P. (1952). *Acta. Cryst.* **5**, 272-276.
Parpaleix, T., Laval, J.M., Majda, M. & Bourdillon, C. (1992) *Anal. Chem.* **64**, 641-646.
Pépy, G. & Kuklin, A. (2001). *Nucl. Inst. Meth. Phys. Res.* B**185**, 198-203.
Porod, G. *Koll. Z.* (1951). **124**, 83-114.
Stefanopoulos, K. L., Romanos, G. E., Mitropoulos, A. C., Kanellopoulos, N. K., Heenan, R. K. (1999). *J. Membrane Sci.* **153**, 1-7.

Received 29 August 2002 • Accepted 2 January 2003